Angular momentum of fission fragments from microscopic theory

Petar Marević, Nicolas Schunck, Jørgen Randrup, and Ramona Vogt

Phys. Rev. C **104**, L021601 — Published 4 August 2021

DOI: 10.1103/PhysRevC.104.L021601

Angular Momentum of Fission Fragments from Microscopic Theory

Petar Marević,[1] Nicolas Schunck,[1] Jørgen Randrup,[2] and Ramona Vogt[1,3]

[1] *Nuclear and Chemical Sciences Division, Lawrence Livermore National Laboratory, Livermore, CA 94551, USA*
[2] *Nuclear Science Division, Lawrence Berkeley National Laboratory, Berkeley, CA 94720, USA*
[3] *Physics and Astronomy Department, University of California, Davis, CA 95616, USA*

(Dated: June 1, 2021)

During nuclear fission, a heavy nucleus splits into two rotating fragments. The associated angular momentum is large, yet the mechanism of its generation and its dependence on the mass of fragments remain poorly understood. In this Letter, we provide the first microscopic calculations of angular momentum distributions in fission fragments for a wide range of fragment masses. For the benchmark case of ^{239}Pu($n_{\rm th}$,f), we find that the angular momentum of the fragments is largely determined by the nuclear shell structure and deformation, and that the heavy fragments therefore typically carry less angular momentum than their light partners. We use the fission model `FREYA` to simulate the emission of neutrons and photons from the fragments. The dependence of the angular momenta on fragment mass after the emission of neutrons and statistical photons is linear for the heavy fragments and either constant or weakly linear for the light fragments, consistent with the universal sawtooth pattern suggested by recent experimental data. Finally, we observe that using microscopic angular momentum distributions modifies the number of emitted photons significantly.

Introduction. — Nuclear fission plays an essential role in fundamental and applied science, but even eighty years after its discovery [1, 2] the microscopic foundation of the phenomenon is yet to be fully understood [3, 4]. In a simple picture, fission can be viewed as the shape evolution of a charged quantum liquid drop that gradually deforms while surmounting multiple potential barriers and finally assumes an extremely deformed shape at scission [5]. Fissionable nuclei predominantly split into two primary fragments that move apart due to the mutual Coulomb repulsion. Simultaneously, primary fragments relax toward their equilibrium shapes and then deexcite by sequential emission of neutrons and photons. The angular momentum (AM) of fission fragments (FFs) influences this deexcitation process, causing the neutron emission to be anisotropic and affecting the number of emitted photons [6–10]. However, the mechanism of the AM generation and its dependence on the mass of fragments are still poorly understood. Very recently, a sawtooth-like mass dependence of the AM suggested in earlier experiments [11] was measured across three different fission reactions [12]. The observed lack of correlation between the AM of the fragment partners was interpreted as a proof of its post-scission origin [12], though it was immediately pointed out that this observation could be explained by a pre-scission mechanism as well [13]. A full understanding of the AM of FFs will eventually need to be rooted in a microscopic framework where the fission phenomenon emerges from internucleon forces and quantum many-body physics. However, such a framework is markedly missing, and the most widely used fission models still rely on AM distributions that are obtained from either statistical or semi-classical methods [10, 14–18].

Currently, nuclear density functional theory (DFT) [19] is the only fully quantum-mechanical approach capable of describing many facets of fission [4, 20]. In particular, DFT models were successfully employed in studies of spontaneous fission half-lives [21], FF mass and charge distributions [22–28], and energy sharing among the FFs [29–32]. There were a few attempts at describing the AM of FFs within the DFT framework, but they either relied on strong and restrictive approximations [33, 34] or were limited to a single pair of fragments only [35]. Consequently, a quantitatively robust and predictive framework for computing AM distributions over the wide range of FF masses that is typically observed in experiments [12, 36, 37] is still missing.

In this Letter, we report the first microscopic calculations of AM distributions in FFs for a wide range of fragment masses. Starting from a large set of extremely deformed scission configurations, projection techniques are employed to extract the AM distributions of 24 fragment pairs in ^{239}Pu($n_{\rm th}$,f). We find that the AM of FFs is largely determined by the underlying shell structure and deformation of fragments at scission. As a result, the heavy FFs typically carry less angular momentum than their light partners. By adapting the fission simulation model `FREYA` to use the microscopic AM distributions, we are able to simulate the emission of neutrons and photons from primary FFs. We find that, after the emission of neutrons and statistical photons, the dependence of the AM on the mass of FFs is linear for the heavy fragments and either constant or weakly linear for the light fragments. This result is consistent with a univeral sawtooth pattern proposed in recent experiments. Finally, we assess the impact of microscopic AM distributions on total neutron and photon multiplicities and find that the latter are significantly modified.

Method. — A set of scission configurations is first determined by solving the Hartree-Fock-Bogoliubov (HFB) equations with the `HFBTHO` package [38], using the SkM* parameterization of the Skyrme energy functional [39]

and a mixed volume-surface contact pairing force [40]. Constraints are imposed on the values of the axially-symmetric quadrupole (q_{20}) and octupole (q_{30}) moments [41], corresponding to the elongation and the reflection asymmetry of the nuclear shape, respectively. In addition, we constrain the expectation value of the neck operator (q_N), which estimates the number of nucleons in a thin neck connecting the two fragments [42]. This approach enables us to explore a three-dimensional $\boldsymbol{q} \equiv (q_{20}, q_{30}, q_N)$ hypersurface in collective space and to generate a large set of scission configurations [43]. A total of 1545 configurations $|\Phi(\boldsymbol{q})\rangle$ in ^{240}Pu are considered, with neck values $1 \leq q_N \leq 3$ and a wide range of quadrupole and octupole deformations; see the Supplemental Material [44] for more details on technical aspects of the HFB calculation and on the properties of scission configurations.

The scission configurations have axially-symmetric densities that are dumbbell-shaped and can readily be divided into heavy ($z < z_N$) and light ($z > z_N$) FFs, where z_N locates the minimum of the density profile. By adapting standard symmetry restoration techniques [45–47] to the case of FFs, AM distributions of the heavy ($F = H$) and the light fragment ($F = L$) for each configuration $|\Phi(\boldsymbol{q})\rangle$ can be calculated as

$$|a_J^F(\boldsymbol{q})|^2 = \int_\beta \langle \Phi(\boldsymbol{q})|\hat{R}_y^F(\beta)|\Phi(\boldsymbol{q})\rangle \,, \tag{1}$$

where $\int_\beta \equiv (J+\frac{1}{2}) \int_0^\pi \, d\beta \sin\beta \, d_{00}^{J*}(\beta)$ denotes integration over the orientation angle β with Wigner matrix elements $d_{00}^J(\beta) = P_J(\cos\beta)$ [48] (P_J is the Legendre polynomial of order J) as weights, and $\hat{R}_y^F(\beta) = \exp(-i\beta\hat{J}_y^F)$ is the rotation operator for fragments. The angular momentum operators $\hat{J}_y^F$ have support within the spatial region $\mathcal{S}^F$ containing each fragment [49, 50]. They are computed from the associated kernels,

$$J_y^F(\boldsymbol{r}, \sigma) = \Theta^{F*}(z - z_N) J_y(\boldsymbol{r}, \sigma) \Theta^F(z - z_N), \tag{2}$$

where $J_y(\boldsymbol{r}, \sigma) = L_y(\boldsymbol{r}) + S_y(\sigma)$ corresponds to the usual angular momentum operator that depends on the spatial coordinates $\boldsymbol{r} \equiv (r_\perp, \phi, z)$ and the spin coordinate σ, $\Theta^H(z - z_N) = 1 - \mathcal{H}(z - z_N)$, $\Theta^L(z - z_N) = \mathcal{H}(z - z_N)$, and $\mathcal{H}(z)$ is the Heaviside step function [51]. The center of mass of each fragment is located at $\boldsymbol{r}_{\rm CM}^F = (0, 0, z_{\rm CM}^F)$. Therefore, we take $\boldsymbol{r} \to \boldsymbol{r} - \boldsymbol{r}_{\rm CM}^F$ in Eq. (2) to determine the angular momentum with respect to the center of mass of each fragment. To ensure a proper convergence of integrals in Eq. (1) for all J values, $N_\beta = 60$ orientation angles are taken into account. Note that the configurations $|\Phi(\boldsymbol{q})\rangle$ are expanded in a basis that is not closed under rotation [52]. Therefore, we must employ the recently introduced technique of symmetry restoration in incomplete bases [53] to evaluate Eq. (1).

The number of nucleons in FFs can be obtained as the integral of the total density over the subspace $\mathcal{S}^F$ containing each fragment. Thus, this calculation represents a mapping of a set of collective variables $\boldsymbol{q}$ in the combined nuclear system (Z, A) onto a set of charges and masses $(Z_F(\boldsymbol{q}), A_F(\boldsymbol{q}))$ in the two fragments. These charges and masses satisfy $Z_H(\boldsymbol{q}) + Z_L(\boldsymbol{q}) = Z$ and $A_H(\boldsymbol{q}) + A_L(\boldsymbol{q}) = A$ but are generally not integers. In principle, one should combine the outlined method with the particle number projection (PNP) in FFs [26, 54, 55], a formidable task that is yet to be undertaken. To extract the desired quantities for integer numbers of nucleons in each fragment, we instead perform a Gaussian Process interpolation [56, 57] over a subset of scission configurations with both the proton and the neutron number in the vicinity of the target values. Therefore, the obtained distributions $|a_J|^2$ are complemented by the corresponding confidence intervals $\sigma(|a_J|^2)$. Finally, the present model is limited to states that obey the natural spin-parity rule, $(-1)^J = \pi$. Consequently, we cannot extract odd J if $q_{30}^F \to 0$ [44]. To account for these rare cases, we solve Eq. (1) for even J, interpolate for odd J, and normalize the entire distribution. This procedure smoothens the distributions of $q_{30}^F \to 0$ configurations while having a negligible effect on the average angular momentum they carry. More details on the entire interpolation procedure can be found in the Supplemental Material [44].

Results. — Starting from a set of 1545 scission configurations, we determined the AM distributions $|a_J^F|^2$ of 24 fragment pairs in ^{239}Pu($n_{\rm th}$,f) within the mass range $126 \leq A_H \leq 150$ ($90 \leq A_L \leq 114$), covering more than 95% of measured mass yields [36, 37]. With a few exceptions, the employed collective space $\boldsymbol{q}$ allows extracting only one Z value per each A (see Figs. 1a and 1b of Ref. [44]). A broader charge dispersion could be obtained by performing the additional PNP in FFs. Furthermore, this initial set comprised a wide range of quadrupole and octupole deformation parameters of the FFs, $\beta_2^F(\boldsymbol{q}) \leq 0.7$ and $|\beta_3^F(\boldsymbol{q})| \leq 0.5$, where $\beta_\lambda^F = (4\pi)/(3A_F R_F^\lambda) q_{\lambda 0}^F$, $q_{\lambda 0}^F$ are the multipole moments [58] of the FFs, and $R_F = 1.2 A_F^{1/3}$ fm. The same Gaussian Process procedure was used to extract these parameters for the integer-valued FFs [44]. We obtained FFs with a wide range of quadrupole deformations and confirmed the findings of Refs. [31, 59] that FFs are octupole-deformed at scission.

Fig. 1a shows the average angular momentum of the heavy and the light primary FFs as a function of their mass number A_F. The average values J_F are obtained from $J_F(J_F + 1) = \sum_{J=0}^{30} J(J + 1)|a_J^F|^2$. The corresponding error bars stem from the Gaussian Process interpolation for integer numbers of nucleons in FFs and they do not represent the total theoretical uncertainty. In particular, another important source of uncertainty is the choice of the energy density functional; the associated uncertainty is likely of the order of $1\hbar$ [35] and may be mass dependent. The heavy FFs display a wide

range of angular momenta and quadrupole deformations that appear to be strongly correlated. The smallest values are found in the region of the doubly magic $^{132}_{50}$Sn nucleus while rare-earth isotopes are highly deformed and on average carry substantial angular momentum. The average values around the most likely fragmentation (A_H:$A_L \approx$ 136:104) are in the range $5-9\,\hbar$. On the other hand, the light FFs are significantly more deformed and therefore on average carry more angular momentum, typically $10-13\,\hbar$. A similar conclusion, but for the most likely fission fragmentation only, was very recently obtained within the framework of time-dependent DFT [35]. These results are at odds with the outputs of the widely-used phenomenological models such as FREYA [10, 14, 15] and CGMF [16–18] where the AM of the FFs is calculated using generic moments of inertia, $\mathcal{I}_F$, that omit important structure and deformation effects. These generic $\mathcal{I}_F$ increase with mass, giving $\mathcal{I}_H > \mathcal{I}_L$, leading to a higher AM for the heavy fragment, $J_H > J_L$. In a separate publication, two of us show that including deformation effects in a phenomenological model indeed reverses this trend [13]. In addition to enabling asymmetric fragmentations by stabilizing octupole deformations [58] and modifying the structure of fission barriers [60], we demonstrate here that the shell effects *at scission* also significantly influence the angular momentum of the fission fragments.

To shed more light on the effect of the underlying shell structure on the angular momentum of primary FFs, we show in Fig. 2a the AM distributions of three fragments in the vicinity of the $Z = 50$ and $N = 82$ magic numbers. Four neutrons away from the double shell closure, $^{128}_{50}$Sn has an average AM of $J_H(\sigma_H^{\rm GP}) \approx 9.2(0.2)\,\hbar$. The situation drastically changes at $N = 82$ where $J_H \approx 2.5(0.1)\,\hbar$ for $^{132}_{50}$Sn. Adding four more nucleons leads to $J_H \approx 6.6(0.3)\,\hbar$ in $^{138}_{54}$Xe. The most advanced microscopic models so far relied on the assumption that FFs can be represented by deformed, isolated nuclei with the same number of nucleons [33, 34]. As shown in the inset of Fig. 2a, these three nuclei are all spherical in their ground states and are thus beyond the scope of models that assume the existence of rigidly deformed equilibria [33]. Considering instead a range of arbitrary deformations around the equilibrium configuration [34] does not yield unique values of angular momenta and consequently provides a very limited predictive capability. In contrast, the present approach considers FFs within the actual combined nuclear system at scission. Consequently, deformations of FFs are automatically determined by the variational principle and are generally different from their equilibrium deformations. This imparts a predictive power to the model and can naturally lead to different AM distributions for FFs with similar equilibrium deformations.

Furthermore, we employed the fission model FREYA to simulate the emission of neutrons and photons from

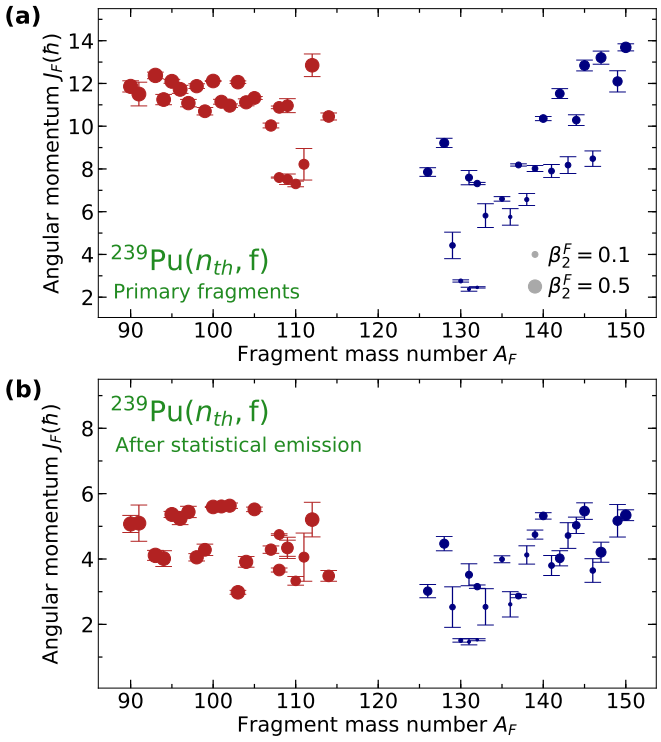

FIG. 1. Average angular momentum J_F of the heavy (blue) and light (red) fission fragments in ^{239}Pu($n_{\rm th}$,f) as a function of their mass number A_F. (a): Average AM of primary fission fragments calculated with microscopic theory. (b): Average AM of the fragments after the emission of neutrons and statistical photons was simulated with FREYA. In both panels, the area of the circles is proportional to the quadrupole deformation parameter β_2^F extracted for the fragments at scission. Note that the legend is illustrative and does not represent two discrete cases. The error bars in both panels represent the $\pm 2\sigma_F^{\rm GP}$ confidence intervals stemming from the Gaussian Process interpolation for integer numbers of nucleons in FFs, where $\sigma_F^{\rm GP} = \sum_J |\frac{\partial J_F(J_F+1)}{\partial |a_J|^2}\sigma(|a_J|^2)|/(2J_F+1)$.

primary FFs and assess the impact of the microscopic AM distributions on neutron and photon multiplicities. FREYA [10, 14, 15] is a Monte Carlo model that generates large samples of complete fission events, providing the full kinematic information for the two product nuclei and the emitted neutrons and photons in each event. Inputs to FREYA are primarily based on experimental data, though a certain degree of modeling is necessary. In particular, FREYA obtains the AM of FFs from a statistical sampling of the dinuclear wriggling and bending modes, employing an adjustable spin temperature T_S [9, 10]. For each fragmentation considered, it is possible to adjust T_S such that the AM distribution generated by FREYA closely matches the one extracted microscopically. Consequently, we can determine the neutron and photon observables resulting from the microscopic AM distributions. For each fragmentation considered, we simulated two hundred thousand fission events and calculated the average angular

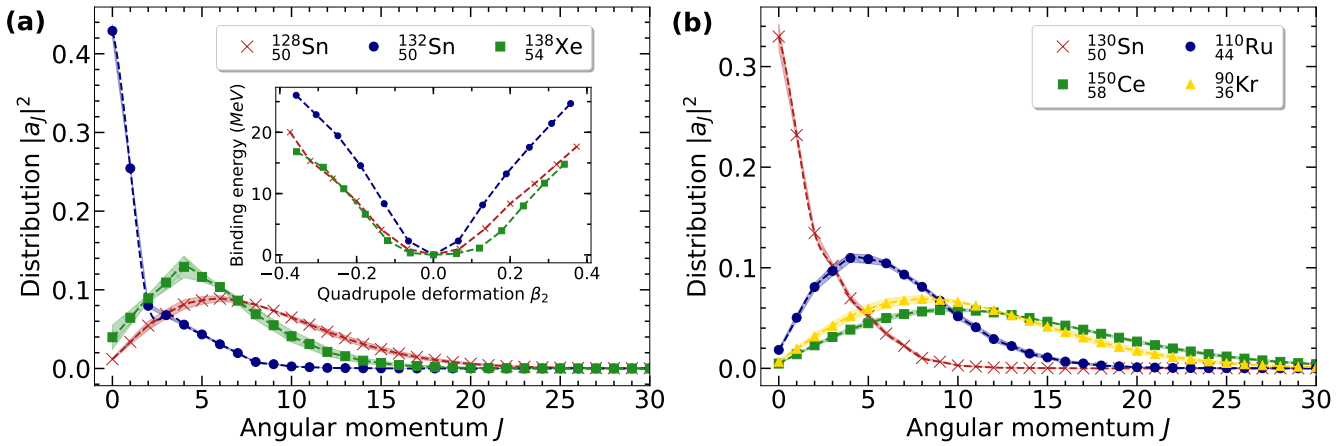

FIG. 2. Angular momentum distributions of primary fission fragments in ^{239}Pu($n_{\rm th}$,f). (a): The distributions for three heavy fragments in the vicinity of the $Z = 50$ and $N = 82$ magic numbers. The inset shows the binding energy of these nuclei (normalized to the corresponding absolute minima) as a function of the quadrupole deformation parameter β_2, calculated with the HFB model. (b): The distributions for the partner fragments from two different mass divisions. In both panels, symbols mark the calculated values and the lines are obtained by a simple spline interpolation. The shaded areas show the $\pm 2\sigma(|a_J|^2)$ confidence intervals from the Gaussian Process interpolation for integer numbers of nucleons in FFs.

momenta after the emission of neutrons and statistical photons (Fig. 1b). The neutron evaporation reduces the average AM only marginally (less than $0.4\hbar$ in each FF), while statistical photons typically remove several units of $\hbar$. Since different FFs can have markedly different AM distributions (Fig. 2b), the angular momentum is not reduced by a constant value. For example, the reduction for the pair of fragments $^{130}_{50}$Sn and $^{110}_{44}$Ru is $\approx 1\hbar$ and $\approx 4\hbar$, respectively. On the other hand, the AM distributions of $^{150}_{58}$Ce and $^{90}_{36}$Kr are more similar and statistical emission reduces their large angular momenta acquired at scission by $\approx 8\hbar$ and $\approx 7\hbar$, respectively. The emission of statistical photons ceases when a nucleus reaches the yrast line and deexcitation to the ground state then proceeds mostly through the emission of quadrupole photons. We compared the average number of neutrons and photons (multiplicities) emitted from each FF during the entire deexcitation process calculated with (i) default `FREYA` AM distributions and (ii) microscopic AM distributions. The neutron multiplicities depend rather weakly on AM distributions, in agreement with the previously reported observation that the rotation of FFs influences the direction of emitted neutrons but not their number [10]. On the other hand, the photon multiplicities are significantly modified, as shown in Table I. In particular, the microscopic calculations yield lower J_H in the vicinity of the double shell closure, leading to lower multiplicities. The trend reverses at larger and smaller A_H, where larger deformations of FFs lead to larger multiplicities. Extending the present model to other fragmentations will enable a full-fledged `FREYA` simulation based on microscopic distributions that can be directly compared with experimental data, ranging between $N_\gamma = 6.88 \pm 0.35$ [61] and $N_\gamma = 7.23 \pm 0.3$ [62].

TABLE I. Total average photon multiplicities N_γ for several fragmentations in ^{239}Pu($n_{\rm th}$,f) calculated with `FREYA`, based on the microscopic DFT or default `FREYA` AM distributions. Mass yields $Y(A_H)$ and charge yields $Y(Z_H)$ (each normalized to 100 for the heavy fragment only) used in `FREYA` [14] give an estimates of the relative importance of each fragmentation.

(Z_H, A_H)	$Y(Z_H)$	$Y(A_H)$	N_γ(DFT)	N_γ(Default)
(50, 128)	2.7	1.04	11.72	8.69
(50, 130)	2.7	2.12	6.35	9.65
(50, 132)	2.7	3.70	4.89	6.62
(54, 138)	15.3	6.09	7.53	7.32
(56, 144)	12.1	4.38	12.46	7.41

Finally, the average angular momenta of FFs in the neutron-induced fission of ^{232}Th and ^{238}U and spontaneous fission of ^{252}Cf were very recently measured at the ALTO facility in Orsay [12]. The authors obtained angular momenta of the FFs after the emission of neutrons and statistical photons (hereafter referred to as the post-emission AM). They inferred the FF angular momenta prior to statistical photon emission by adding a constant $1\hbar$ shift, according to the prescription of Ref. [63]. The post-emission AM in all three reactions are in the $J_{H,L} \approx 3 - 7\hbar$ range and exhibit a sawtooth mass dependence which is proposed to be universal. Our calculated post-emission AM in ^{239}Pu($n_{\rm th}$,f) (Fig. 1b) are in a very similar range, but the impact of statistical photons is markedly larger and more complex than the constant $1\hbar$ shift adopted in [12]. The $J_H(A_H)$ values calculated both before and after the emission of statistical photons are consistent with the proposed linear mass dependence. On the other hand, while the post-emission $J_L(A_L)$ val-

ues are not incompatible with a weak linear dependence, they appear more consistent with a horizontal line. The overall pattern we observe is consistent with the proposed universal sawtooth pattern. In addition, we stress that we typically do observe asymmetries in the AM of partner primary fragments. In particular, a light fragment typically carries more AM than its heavy counterpart (for example, $7.3(0.1)\hbar$ in $^{110}_{44}$Ru and $2.8(0.1)\hbar$ in $^{130}_{50}$Sn), but the opposite is also possible ($13.7(0.2)\hbar$ in $^{150}_{58}$Ce and $11.9(0.3)\hbar$ in $^{90}_{36}$Kr). This invalidates the claim from [12] that models based on the angular momentum generation at scission due to the deformation of FFs cannot account for such asymmetries.

Conclusion. — We have presented the first microscopic calculation of angular momentum distributions for a wide range of fission fragment masses. These calculations reveal the large impact of the underlying shell structure of the fission fragments at scission on their angular momentum. The average angular momenta of the primary fission fragments exhibit a marked dip near the doubly magic fragment ^{132}Sn and the resulting mass dependence is reminiscent of the recently observed sawtooth pattern [12]. The present work demonstrates the importance of using a predictive theory to compute properties that can vary significantly from one fragmentation to the next and which could thus provide valuable guidance for nuclear data evaluation. This novel treatment may also be useful for describing the properties of fragments in very neutron-rich nuclei, such as those involved in nucleosynthesis processes, where experimental data are unavailable.

Acknowledgements. — P. M. and N. S. acknowledge stimulating discussions with Marc Verrière and David Regnier. R. V. thanks Robert V. F. Janssens for discussion. This work was performed under the auspices of the U.S. Department of Energy by Lawrence Livermore National Laboratory under Contract DE-AC52-07NA27344 and under the NUCLEI SciDAC-4 collaboration. J. R. acknowledges support from the Office of Nuclear Physics in the U.S. Department of Energy under Contracts DE-AC02-05CH11231. Computing support for this work came from the Lawrence Livermore National Laboratory (LLNL) Institutional Computing Grand Challenge program.

[1] O. Hahn and F. Strassmann. Über den Nachweis und das Verhalten der bei der Bestrahlung des Urans mittels Neutronen entstehenden Erdalkalimetalle. *Naturwissenschaften*, 27:11–15, 1939.

[2] L. Meitner and O. R. Frisch. Disintegration of Uranium by Neutrons: a New Type of Nuclear Reaction. *Nature (London)*, 143:239, 1939.

[3] H. J. Krappe and K. Pomorski. *Theory of Nuclear Fission.* Springer, 2012.

[4] M. Bender et al. Future of nuclear fission theory. *Journal of Physics G: Nuclear and Particle Physics*, 47(11):113002, 2020.

[5] N. Bohr and J. A. Wheeler. The Mechanism of Nuclear Fission. *Phys. Rev.*, 56(5):426, 1939.

[6] H. R. Bowman, S. G. Thompson, J. C. D. Milton, and W. J. Swiatecki. Velocity and Angular Distributions of Prompt Neutrons from Spontaneous Fission of Cf^{252}. *Phys. Rev.*, 126:2120–2136, 1962.

[7] A. Gavron. Angular distribution of neutrons from fission fragments. *Phys. Rev. C*, 13:2562–2563, 1976.

[8] J. S. Pringle and F. D. Brooks. Angular Correlation of Neutrons from Spontaneous Fission of ^{252}Cf. *Phys. Rev. Lett.*, 35:1563–1566, 1975.

[9] R. Vogt and J. Randrup. Improved modeling of photon observables with the event-by-event fission model FREYA. *Phys. Rev. C*, 96:064620, 2017.

[10] R. Vogt and J. Randrup. Angular momentum effects in fission. *Phys. Rev. C*, 103:014610, 2021.

[11] H. Naik, S. P. Dange, and R. J. Singh. Angular momentum of fission fragments in low energy fission of actinides. *Phys. Rev. C*, 71(1):014304, 2005.

[12] J. N. Wilson et al. Angular momentum generation in nuclear fission. *Nature*, 590:566–570, 2021.

[13] J. Randrup and R. Vogt. Generation of fragment angular momentum in fission. *arXiv:2103.14778*, 2021.

[14] J. M. Verbeke, J. Randrup, and R. Vogt. Fission Reaction Event Yield Algorithm FREYA 2.0.2. *Computer Physics Communications*, 222:263 – 266, 2018.

[15] J. Randrup and R. Vogt. Refined treatment of angular momentum in the event-by-event fission model FREYA. *Phys. Rev. C*, 89:044601, 2014.

[16] P. Talou, B. Becker, T. Kawano, M. B. Chadwick, and Y. Danon. Advanced Monte Carlo modeling of prompt fission neutrons for thermal and fast neutron-induced fission reactions on ^{239}Pu. *Phys. Rev. C*, 83:064612, 2011.

[17] B. Becker, P. Talou, T. Kawano, Y. Danon, and I. Stetcu. Monte Carlo Hauser-Feshbach predictions of prompt fission γ rays: Application to $n_{\rm th} + ^{235}$U, $n_{\rm th} + ^{239}$Pu, and ^{252}Cf (sf). *Phys. Rev. C*, 87:014617, 2013.

[18] I. Stetcu, P. Talou, and T. Kawano. Neutron-induced fission: properties of prompt neutron and γ rays as a function of incident energy. *EPJ Web of Conferences*, 122:01012, 2016.

[19] N. Schunck. *Energy Density Functional Methods for Atomic Nuclei.* IOP Expanding Physics. IOP Publishing, Bristol, UK, 2019. OCLC: 1034572493.

[20] N. Schunck and L. M. Robledo. Microscopic Theory of Nuclear Fission: A Review. *Rep. Prog. Phys.*, 79(11):116301, 2016.

[21] A. Baran, M. Kowal, P.-G. Reinhard, L. M. Robledo, A. Staszczak, and M. Warda. Fission barriers and probabilities of spontaneous fission for elements with $Z \geq 100$. *Nucl. Phys. A*, 944:442, 2015.

[22] H. Goutte, P. Casoli, and J.-F. Berger. Mass and kinetic energy distributions of fission fragments using the time dependent generator coordinate method. *Nucl. Phys. A*, 734:217, 2004.

[23] D. Regnier, N. Dubray, N. Schunck, and M. Verrière. Fission fragment charge and mass distributions in ^{239}Pu(n,f) in the adiabatic nuclear energy density functional theory. *Phys. Rev. C*, 93(5):054611, 2016.

[24] H. Tao, J. Zhao, Z. P. Li, T. Nikšić, and D. Vretenar. Microscopic study of induced fission dynamics of ^{226}Th

with covariant energy density functionals. *Phys. Rev. C*, 96(2):024319, 2017.

[25] D. Regnier, N. Dubray, and N. Schunck. From asymmetric to symmetric fission in the fermium isotopes within the time-dependent generator-coordinate-method formalism. *Phys. Rev. C*, 99(2):024611, 2019.

[26] M. Verrière, N. Schunck, and T. Kawano. Number of particles in fission fragments. *Phys. Rev. C*, 100(2):024612, 2019.

[27] J. Zhao, T. Nikšić, D. Vretenar, and S. G. Zhou. Microscopic self-consistent description of induced fission dynamics: Finite-temperature effects. *Phys. Rev. C*, 99(1):014618, 2019.

[28] J. Zhao, J. Xiang, Z. P. Li, T. Nikšić, D. Vretenar, and S. G. Zhou. Time-dependent generator-coordinate-method study of mass-asymmetric fission of actinides. *Phys. Rev. C*, 99(5):054613, 2019.

[29] W. Younes and D. Gogny. Nuclear Scission and Quantum Localization. *Phys. Rev. Lett.*, 107(13):132501, 2011.

[30] C. Simenel and A. S. Umar. Formation and dynamics of fission fragments. *Phys. Rev. C*, 89:031601, 2014.

[31] A. Bulgac, P. Magierski, K. J. Roche, and I. Stetcu. Induced Fission of ^{240}Pu within a Real-Time Microscopic Framework. *Phys. Rev. Lett.*, 116(12):122504, 2016.

[32] A. Bulgac, S. Jin, K. J. Roche, N. Schunck, and I. Stetcu. Fission dynamics of ^{240}Pu from saddle to scission and beyond. *Phys. Rev. C*, 100(3):034615, 2019.

[33] L. Bonneau, P. Quentin, and I. N. Mikhailov. Scission configurations and their implication in fission-fragment angular momenta. *Phys. Rev. C*, 75:064313, 2007.

[34] G. F. Bertsch, T. Kawano, and L. M. Robledo. Angular momentum of fission fragments. *Phys. Rev. C*, 99:034603, 2019.

[35] A. Bulgac, I. Abdurrahman, S. Jin, K. Godbey, N. Schunck, and I Stetcu. Fission fragments intrinsic spins and their correlations. *arXiv:2012.13422*, 2020.

[36] P. Schillebeeckx, C. Wagemans, A. J. Deruytter, and R. Barthélémy. Comparative study of the fragments' mass and energy characteristics in the spontaneous fussion of ^{238}Pu, ^{240}Pu and ^{242}Pu and in the thermal-neutron-induced fission of ^{239}Pu. *Nuclear Physics A*, 545(3):623 – 645, 1992.

[37] K. Nishio, Y. Nakagome, I. Kanno, and I. Kimura. Measurement of Fragment Mass Dependent Kinetic Energy and Neutron Multiplicity for Thermal Neutron Induced Fission of Plutonium-239. *Journal of Nuclear Science and Technology*, 32(5):404–414, 1995.

[38] R. Navarro Perez, N. Schunck, R.-D. Lasseri, C. Zhang, and J. Sarich. Axially deformed solution of the Skyrme–Hartree–Fock–Bogolyubov equations using the transformed harmonic oscillator basis (III) HFBTHO (v3.00): A new version of the program. *Comput. Phys. Commun.*, 220(Supplement C):363, 2017.

[39] J. Bartel, P. Quentin, M. Brack, C. Guet, and H.-B. Håkansson. Towards a better parametrisation of Skyrme-like effective forces: A critical study of the SkM force. *Nucl. Phys. A*, 386(1):79, 1982.

[40] J. Dobaczewski, W. Nazarewicz, and M. V. Stoitsov. Contact Pairing Interaction for the Hartree-Fock-Bogoliubov Calculations. In *The Nuclear Many-Body Problem 2001*, number 53 in Nato Science Series II, page 181. Springer Netherlands, 2002.

[41] J. Dobaczewski and P. Olbratowski. Solution of the Skyrme–Hartree–Fock–Bogolyubov equations in the Cartesian deformed harmonic-oscillator basis. (IV) HFODD (v2.08i): a new version of the program. *Computer Physics Communications*, 158(3):158 – 191, 2004.

[42] W. Younes and D. Gogny. Microscopic calculation of ^{240}Pu scission with a finite-range effective force. *Phys. Rev. C*, 80:054313, 2009.

[43] N. Schunck, D. Duke, H. Carr, and A. Knoll. Description of induced nuclear fission with Skyrme energy functionals: Static potential energy surfaces and fission fragment properties. *Phys. Rev. C*, 90(5):054305, 2014.

[44] See Supplemental Material at [URL will be inserted by publisher] for more details on generating scission configurations and extracting angular momentum distributions and deformation parameters for integer number of nucleons in the fission fragments.

[45] P. Ring and P. Schuck. *The Nuclear Many-Body Problem*. Texts and Monographs in Physics. Springer, 2004.

[46] J. A. Sheikh, J. Dobaczewski, P. Ring, L. M. Robledo, and C. Yannouleas. Symmetry Restoration in Mean-Field Approaches. *arXiv:1901.06992*, 2019.

[47] B. Bally and M. Bender. Projection on particle number and angular momentum: Example of triaxial Bogoliubov quasiparticle states. *Phys. Rev. C*, 103:024315, 2021.

[48] D. A. Varshalovich, A. N. Moskalev, and V. K. Khersonskii. *Quantum Theory of Angular Momentum*. World Scientific, Singapore, 1988.

[49] K. Sekizawa and K. Yabana. Particle-number projection method in time-dependent Hartree-Fock theory: Properties of reaction products. *Phys. Rev. C*, 90:064614, 2014.

[50] K. Sekizawa. Microscopic description of production cross sections including deexcitation effects. *Phys. Rev. C*, 96:014615, 2017.

[51] M. Abramowitz and I. A. Stegun. *Handbook of Mathematical Functions: With Formulas, Graphs, and Mathematical Tables*. Dover Books on Advanced Mathematics, Dover Publications, New York, 1965.

[52] L. M. Robledo. Practical formulation of the extended Wick's theorem and the Onishi formula. *Phys. Rev. C*, 50(6):2874, 1994.

[53] P. Marević and N. Schunck. Fission of ^{240}Pu with Symmetry-Restored Density Functional Theory. *Phys. Rev. Lett.*, 125:102504, 2020.

[54] G. Scamps and Y. Hashimoto. Transfer probabilities for the reactions ^{14,20}O+^{20}O in terms of multiple time-dependent Hartree-Fock-Bogoliubov trajectories. *Phys. Rev. C*, 96:031602, 2017.

[55] A. Bulgac. Projection of good quantum numbers for reaction fragments. *Phys. Rev. C*, 100:034612, 2019.

[56] C. E. Rasmussen and C. K. I. Williams. *Gaussian Processes for Machine Learning*. Adaptive Computation and Machine Learning. MIT Press, Cambridge, MA, USA, 2006.

[57] F. Pedregosa, G. Varoquaux, A. Gramfort, V. Michel, B. Thirion, O. Grisel, M. Blondel, P. Prettenhofer, R. Weiss, V. Dubourg, J. Vanderplas, A. Passos, D. Cournapeau, M. Brucher, M. Perrot, and E. Duchesnay. Scikit-learn: Machine learning in Python. *Journal of Machine Learning Research*, 12:2825–2830, 2011.

[58] G. Scamps and C. Simenel. Impact of pear-shaped fission fragments on mass-asymmetric fission in actinides. *Nature*, 564 (7736):382–385, 2019.

[59] G. Scamps and C. Simenel. Effect of shell structure on the fission of sub-lead nuclei. *Phys. Rev. C*, 100(4):041602, 2019.

[60] M. Brack, J. Damgaard, A. S. Jensen, H. C. Pauli, V. M. Strutinsky, and C. Y. Wong. Funny Hills: The Shell-Correction Approach to Nuclear Shell Effects and Its Applications to the Fission Process. *Rev. Mod. Phys.*, 44:320–405, 1972.

[61] F. Pleasonton. Prompt gamma-rays emitted in the thermal-neutron induced fission of ^{233}U and ^{239}Pu. *Nuclear Physics A*, 213(2):413 – 425, 1973.

[62] V. V. Verbinski, H. Weber, and R. E. Sund. Prompt gamma rays from ^{235}U(n, f), ^{239}Pu(n, f), and spontaneous fission of ^{252}Cf, 1973.

[63] Y. Abdelrahman, J. L. Durell, W. Gelletly, W. R. Phillips, I. Ahmad, R. Holzmann, R. V. F. Janssens, T. L. Khoo, W. C. Ma, and M. W. Drigert. Average spins of primary fission fragments. *Physics Letters B*, 199(4):504–508, 1987.